Atomic structure in magnetic cluster assembled Fe/Co films as determined from extended absorption fine structure

2006 J. Phys.: Condens. Matter 18 2385

(http://iopscience.iop.org/0953-8984/18/8/004)

INSTITUTE OF PHYSICS PUBLISHING JOURNAL OF PHYSICS: CONDENSED MATTER

J. Phys.: Condens. Matter **18** (2006) 2385–2399 doi:10.1088/0953-8984/18/8/004

Atomic structure in magnetic cluster assembled Fe/Co films as determined from extended absorption fine structure

S H Baker[1,3], M Roy[1], S Louch[2] and C Binns[1]

[1] Department of Physics and Astronomy, University of Leicester, Leicester LE1 7RH, UK
[2] The Centre for Process Innovation, Functional Materials, Wilton Centre, Wilton, Redcar TS10 4RF, UK

E-mail: bak@le.ac.uk

Received 30 September 2005
Published 10 February 2006
Online at stacks.iop.org/JPhysCM/18/2385

Abstract

The atomic structure of nanocomposite Fe/Co films has been studied using synchrotron radiation. Films in which Co nanoclusters are embedded in an Fe matrix, and films where Fe nanoclusters are embedded in Co, are both investigated. The samples were prepared by co-deposition using a gas aggregation cluster source. Co and Fe K edge EXAFS measurements were used to probe the atomic structure within the Co and Fe nanoclusters respectively as a function of cluster volume filling fraction. In an Fe matrix, the Co clusters are found to adopt a bcc structure across the composition range investigated; at the highest cluster filling fraction of nearly 40%, the atomic structure still does not revert to hcp, the crystal structure in bulk Co. Fe nanoclusters embedded in Co retain the bcc structure of bulk Fe.

1. Introduction

Nanosized clusters of magnetic materials such as Fe and Co display novel properties as distinct from the bulk material, which include enhanced atomic magnetic moments. This is true not only for free clusters, where the magnetic moments can be measured in Stern–Gerlach experiments [1], but also for clusters supported on a substrate, for which the moments can be measured by x-ray magnetic circular dichroism (XMCD) [2, 3]. The experimental confirmation of enhanced moments in magnetic nanoclusters has led to much recent effort to produce 'new' magnetic materials assembled from clusters. A convenient way to prepare cluster-assembled materials is by co-deposition from an intense size-selected cluster beam and a molecular beam of another material. This produces a three-dimensional assembly in which clusters are embedded in a matrix of another material, which itself can be magnetic. It also allows *independent* control over the cluster volume filling fraction and cluster size.

[3] Author to whom any correspondence should be addressed.

Novel behaviour in magnetic nanoclusters is due in part to a high proportion of atoms at the cluster surface; these have a reduced coordination, which causes a narrowing of the valence d bands and an increase in density of states at the Fermi level. This increases the spin magnetic moment towards the high-spin atomic limit [1, 4]. The orbital magnetic moment is also increased as a result of spin–orbit coupling; in addition, the reduced symmetry in a cluster leads to less effective quenching of the orbital magnetism by the crystal field. Further contributions to novel effects in magnetic nanoclusters come from the quantum size effect [5, 6] and modified electron screening behaviour.

The atomic structure within nanoclusters is also expected to play an important role in determining their electronic and magnetic properties, as in ultra-thin Fe films [7, 8]. As well as a possible size dependence, in the case of embedded clusters the matrix material may also affect the structure in the clusters [9]. A knowledge of the intra-cluster atomic structure is therefore important in magnetic cluster-assembled materials.

Extended absorption fine structure (EXAFS) measurements are a powerful element-specific probe of the interatomic structure in nanocomposite materials. Previous work on magnetic nanocomposite materials includes a number of reports where EXAFS has been used to investigate the structure of magnetic clusters embedded in non-magnetic matrices. In granular Fe/Cu films, Fe K edge EXAFS measurements have shown that the Fe clusters adopt a face centred cubic (fcc) structure for Fe concentrations less than 22 at.% but revert to a bulk body centred cubic (bcc) structure above 35 at.% [10]. In a Ag matrix, Fe clusters retain a bcc structure [9, 10] while in amorphous carbon (a-C) there is evidence for both fcc and bcc structures in the clusters [9]. A distorted fcc structure is observed in columnar-like Fe islands, grown on N_2-dosed Cu(100) [11]. Co K edge EXAFS experiments performed on melt-spun Co_xCu_{1-x} ribbons [12–14] indicate the formation of fcc Co granules, correlated with the evolution in superparamagnetic behaviour observed in magnetization measurements [14]. EXAFS measurements on Co clusters prepared by chemical methods suggest the existence of disordered grain boundaries in the nanocrystalline structure [15]. Mixed Co–Ag clusters are expected to have a core–shell structure, with an Ag shell surrounding a Co core, due to the immiscibility of Co and Ag; Co edge EXAFS on these clusters, when embedded in MgO, show that some Co atoms are in contact with those of the matrix, indicating that the Ag shell is not perfect [16]. In addition to nanoclusters of magnetic materials, EXAFS techniques have been used to investigate the structure in nanoclusters of e.g. Au [17, 18], Pt [19] and Pd–Au [20], which are important for catalysis applications.

In this paper, we present the results of EXAFS experiments, which were carried out in order to investigate the atomic structure in magnetic cluster-assembled Fe/Co films. The structure of Fe nanoclusters embedded in a Co matrix, and that of Co clusters in an Fe matrix, were both studied as a function of composition. Magnetometry measurements on these samples will be reported elsewhere [21].

2. Experimental details

The nanocomposite Fe/Co samples were prepared in the form of thin films by codeposition onto Si(100) substrates using a gas aggregation cluster source [22] and a molecular beam epitaxy (MBE) source. Deposition rates of the clusters and the matrix material (deposited from the MBE source) at the substrate were measured by means of a quartz crystal thickness monitor; hence, we were able to control the volume filling fraction (VFF) of clusters within the film by choosing the deposition rates appropriately. The film compositions varied from ∼5% VFF (isolated clusters) through to 100% VFF (pure cluster films). For the purposes of comparison, 500 Å films of Fe and Co were also grown using the MBE sources. In all cases, a

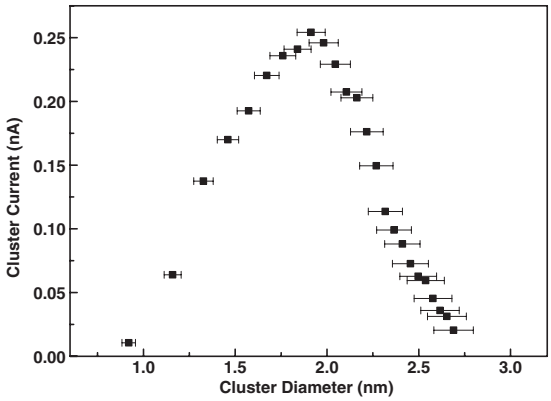

Figure 1. Size distribution of Co clusters typically produced in the gas aggregation cluster source, measured with the quadrupole filter operating at a size resolution of ±4%.

150 Å buffer and 400 Å capping layer of Ag were deposited (from an MBE source) in order to protect the films against oxidation after removal from the deposition chamber.

A detailed description of the cluster source is given elsewhere [22]. In brief, it is ultra-high-vacuum compatible with contaminant partial pressures of CO and H_2O less than 4×10^{-10} mbar during deposition. The base pressure in the deposition chamber is 2×10^{-10} mbar or better. The cluster source produces a log-normal distribution of cluster sizes, with a most probable cluster size of ∼2 nm. An axially mounted quadrupole filter allows *in situ* monitoring of the size distribution of deposited clusters (shown in figure 1).

The atomic structure within the Fe and Co clusters was probed by means of Fe K edge and Co K edge EXAFS experiments respectively, at the Synchrotron Radiation Source at Daresbury Laboratory. All measurements were performed on beamline 7.1, with a double-crystal Si(111) monochromator. Harmonic rejection was set at 70% by detuning the monochromator, and the incident x-ray intensity was measured using an ionization chamber containing an Ar/He gas mixture. The Fe and Co edge absorption spectra $\mu(E)$ were measured in fluorescence with a nine-element monolithic Ge detector.

The measured absorption spectra $\mu(E)$ were background-subtracted and normalized using the Daresbury program EXBACK, which fits low order polynomials to the smoothly varying background absorption. This yields the EXAFS spectra $\chi(E)$. These could then be analysed to obtain experimental values for structural parameters such as the bond lengths r_j, the mean square variations in bond length σ_j^2 (Debye–Waller factor) and coordination numbers N_j by fitting the experimental $\chi(E)$ to calculated EXAFS functions. This was achieved with the program EXCURV98 [23], which uses Hedin–Lundqvist potentials to calculate the scattering phase shifts and also uses the fast curved-wave theory of Gurman *et al* [24] to calculate $\chi(E)$. All errors are quoted to plus or minus two standard deviations.

3. Results

3.1. Fe and Co MBE films

Figure 2 shows the EXAFS χ (weighted by k^3) and associated Fourier transform for the Fe MBE film, where k is the photoelectron wavevector. A good fit to the data was obtained with four statistically significant shells, and was entirely consistent with the bcc structure. In the fit, the coordinations N_j were fixed at the values associated with bcc, the structure at room

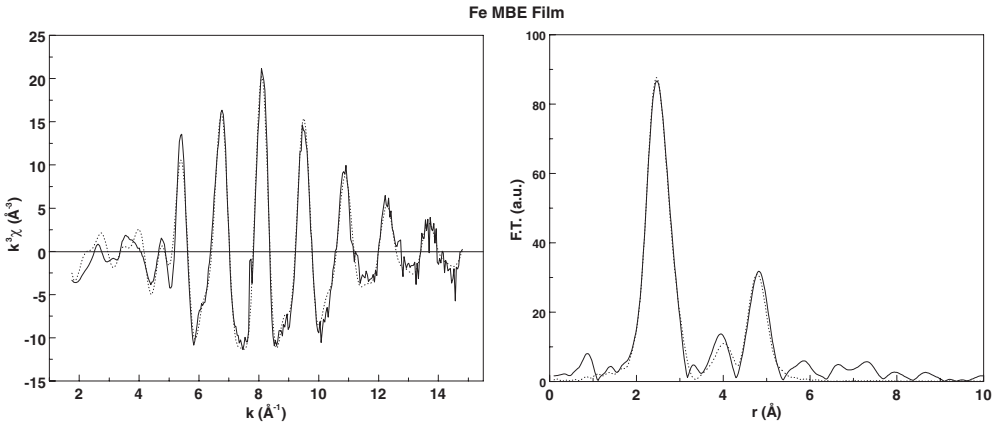

Figure 2. EXAFS spectrum χ (weighted by k^3) plotted as a function of photoelectron wavevector k, and associated Fourier transform (FT), for Fe film grown by MBE.

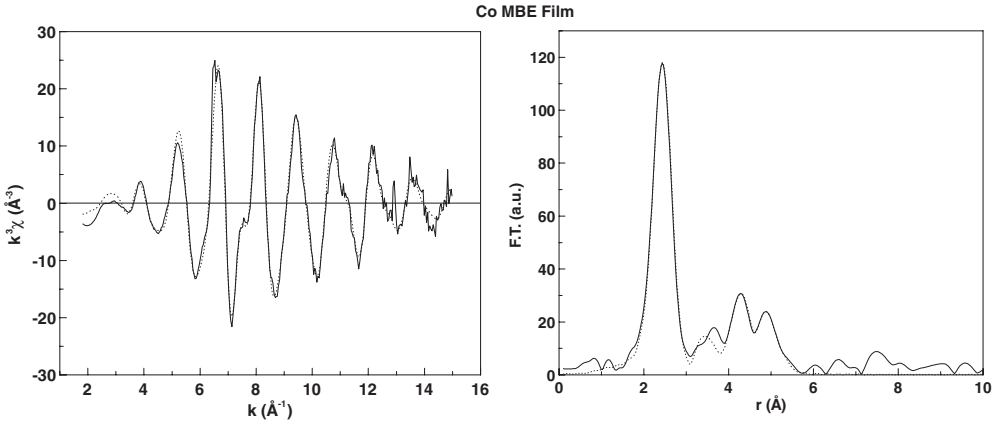

Figure 3. EXAFS spectrum $k^3\chi$ and Fourier transform for Co film grown by MBE.

temperature of bulk Fe, while the interatomic distances r_j and Debye–Waller factors σ_j^2 were allowed to vary freely. The fitted values of r_j and σ_j^2 are listed in table 1, along with the interatomic distances and coordinations in bulk bcc Fe.

The k^3-weighted EXAFS, $k^3\chi$, and Fourier transform for the Co MBE film are given in figure 3. The fit to the data was consistent with hcp, the structure adopted by bulk Co. It was possible to fit six statistically significant shells, and the values of r_j and σ_j^2 obtained can be found in table 1. The interatomic distances and coordinations in bulk Co are also given in the table. As for the Fe film, N_j were fixed during the fit at the values associated with the bulk material. The analysis program allows multiple scattering effects to be included. In the fit here, we allowed for multiple scattering between shells 1 and 6, as expected in hcp structures.

3.2. Co clusters in Fe

Figure 4 shows the Co K edge EXAFS and Fourier transform for a sample containing 28.5% VFF of Co clusters in an Fe matrix. Qualitatively, they look different to the spectra for the Co MBE film but similar to those for the Fe MBE film. This is reinforced by the data analysis

Table 1. Structural parameters r_j, $2\sigma_j^2$ (interatomic distance, Debye–Waller factor respectively) obtained from fits to the EXAFS for MBE Fe and Co films. Also included are the interatomic distances and coordinations N_j for bcc Fe and hcp Co.

	Shell 1	Shell 2	Shell 3	Shell 4	Shell 5	Shell 6
MBE Fe film	$r_1 = 2.50 \pm 0.01$ Å $2\sigma_1^2 = 0.013 \pm 0.001$ Å^2	$r_2 = 2.86 \pm 0.01$ Å $2\sigma_2^2 = 0.024 \pm 0.002$ Å^2	$r_3 = 4.12 \pm 0.02$ Å $2\sigma_3^2 = 0.030 \pm 0.004$ Å^2	$r_4 = 4.81 \pm 0.01$ Å $2\sigma_4^2 = 0.018 \pm 0.001$ Å^2		
bcc Fe	$r_1 = 2.49$ Å $N_1 = 8$	$r_2 = 2.87$ Å $N_2 = 6$	$r_3 = 4.06$ Å $N_3 = 12$	$r_4 = 4.76$ Å $N_4 = 24$	$r_5 = 4.97$ Å $N_5 = 8$	
MBE Co film	$r_1 = 2.50 \pm 0.01$ Å $2\sigma_1^2 = 0.013 \pm 0.001$ Å^2	$r_2 = 3.52 \pm 0.02$ Å $2\sigma_2^2 = 0.022 \pm 0.003$ Å^2	$r_3 = 4.03 \pm 0.04$ Å $2\sigma_3^2 = 0.015 \pm 0.007$ Å^2	$r_4 = 4.36 \pm 0.01$ Å $2\sigma_4^2 = 0.019 \pm 0.002$ Å^2	$r_5 = 4.85 \pm 0.01$ Å $2\sigma_5^2 = 0.014 \pm 0.002$ Å^2	$r_6 = 5.19 \pm 0.03$ Å $2\sigma_6^2 = 0.027 \pm 0.007$ Å^2
hcp Co	$r_1 = 2.50$ Å[a] $N_1 = 12$[a]	$r_2 = 3.54$ Å $N_2 = 6$	$r_3 = 4.07$ Å $N_3 = 2$	$r_4 = 4.34$ Å $N_4 = 18$	$r_5 = 4.78$ Å $N_5 = 12$	$r_6 = 5.01$ Å $N_6 = 6$

[a] The first shell in hcp Co is actually split, with six atoms at 2.497 Å and six atoms at 2.507 Å. The experimental errors do not allow us to resolve these.

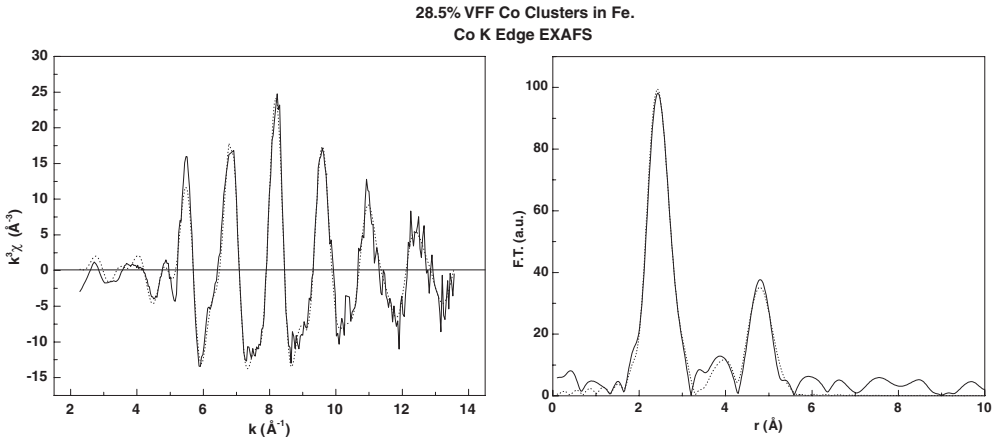

Figure 4. Co K edge EXAFS spectrum $k^3\chi$ and Fourier transform for Co clusters in a film containing 28.5% VFF Co clusters embedded in an Fe matrix.

which yields a fit consistent with the bcc structure. During the fitting procedure, N_j were held fixed at bulk bcc values. Table 2 gives the values of r_j and σ_j^2 for this sample. Comparison of these with the interatomic distances in bcc Fe, also given in table 2, indicates that the lattice parameter for the Co clusters is slightly reduced relative to that for bulk Fe. Allowing N_j to vary freely in the fit does not within experimental error affect the values of r_j, and the bulk values for N_j are included within the experimental uncertainties obtained for N_j.

Table 3 gives the fitted values of r_j and σ_j^2 obtained from the Co edge EXAFS for all the Co cluster/Fe samples. Across the composition range investigated, the fits to the data are all clearly consistent with a bcc structure in the Co clusters. It was possible to fit either four or five statistically significant shells; where five shells were fitted, multiple scattering effects were accounted for between shells one and five, as expected in the bcc structure. For a pure Co cluster film, however, the EXAFS looked very similar to the data in figure 3 for the Co MBE film and analysis confirmed that the structure was hcp.

As we have noted previously [9], the Debye–Waller factors tend to increase with increasing shell radius. This can be interpreted as being due to correlations in the thermal motions of the near neighbours [25].

The Fe K edge EXAFS data for the 28.5% VFF. Co cluster/Fe sample is given in figure 5. Qualitatively, they look similar to the data in figure 2 for the bcc Fe MBE film. Table 4 gives the fitted values of r_j and σ_j^2 obtained from analysis of the Fe edge EXAFS for all the Co cluster/Fe samples. Five shell fits were obtained in all cases. The fit parameters in table 4 were obtained with N_j held fixed during the fitting at bulk bcc values. As for the Co edge data, allowing N_j to vary in the fits did not affect the fitted values of r_j, and the (sometimes large) experimental uncertainties in N_j generally included the bulk values. It is clear that the Fe matrix maintains the bulk bcc structure across the composition range investigated.

3.3. Fe clusters in Co

Figure 6 shows the Fe K edge EXAFS data for the 9.1% VFF Fe cluster/Co film. It is similar in appearance to the Fe MBE film data in figure 2. In all cases, fits to the data with four or five statistically significant shells were possible. Table 5 lists the fit parameters obtained. Comparison of these with the interatomic distances in bulk Fe (table 1) show that, across the

Table 2. Structural parameters r_j, $2\sigma_j^2$ (interatomic distance, Debye–Waller factor respectively) obtained from fits to the Co K edge EXAFS for a film containing 28.5% VFF of Co clusters embedded in Fe. The coordinations N_i were fixed at values associated with the bcc structure. Also reproduced are the interatomic distances and coordinations of bcc Fe.

	Shell 1	Shell 2	Shell 3	Shell 4	Shell 5
28.5% VFF Co/Fe	$r_1 = 2.45 \pm 0.01$ Å $2\sigma_1^2 = 0.011 \pm 0.001$ Å^2 ($N_1 = 8$)	$r_2 = 2.84 \pm 0.02$ Å $2\sigma_2^2 = 0.023 \pm 0.003$ Å^2 ($N_2 = 6$)	$r_3 = 4.05 \pm 0.02$ Å $2\sigma_3^2 = 0.027 \pm 0.004$ Å^2 ($N_3 = 12$)	$r_4 = 4.73 \pm 0.02$ Å $2\sigma_4^2 = 0.024 \pm 0.004$ Å^2 ($N_4 = 24$)	$r_5 = 4.94 \pm 0.02$ Å $2\sigma_5^2 = 0.021 \pm 0.003$ Å^2 ($N_5 = 8$)
bcc Fe	$r_1 = 2.49$ Å $N_1 = 8$	$r_2 = 2.87$ Å $N_2 = 6$	$r_3 = 4.06$ Å $N_3 = 12$	$r_4 = 4.76$ Å $N_4 = 24$	$r_5 = 4.97$ Å $N_5 = 8$

Table 3. Structural parameters $r_j, 2\sigma_j^2$ (interatomic distance, Debye–Waller factor respectively) obtained from fits to the Co K edge EXAFS for films of Co clusters embedded in Fe. The coordinations were fixed at values associated with the bcc structure.

	Shell 1	Shell 2	Shell 3	Shell 4	Shell 5
4.9% VFF Co/Fe	$r_1 = 2.45 \pm 0.01$ Å $2\sigma_1^2 = 0.009 \pm 0.002$ Å^2	$r_2 = 2.85 \pm 0.02$ Å $2\sigma_2^2 = 0.016 \pm 0.005$ Å^2	$r_3 = 4.06 \pm 0.03$ Å $2\sigma_3^2 = 0.022 \pm 0.007$ Å^2	$r_4 = 4.75 \pm 0.02$ Å $2\sigma_4^2 = 0.011 \pm 0.003$ Å^2	
7.0% VFF Co/Fe	$r_1 = 2.45 \pm 0.01$ Å $2\sigma_1^2 = 0.010 \pm 0.001$ Å^2	$r_2 = 2.86 \pm 0.01$ Å $2\sigma_2^2 = 0.018 \pm 0.002$ Å^2	$r_3 = 4.06 \pm 0.02$ Å $2\sigma_3^2 = 0.020 \pm 0.003$ Å^2	$r_4 = 4.71 \pm 0.02$ Å $2\sigma_4^2 = 0.022 \pm 0.003$ Å^2	$r_5 = 4.94 \pm 0.02$ Å $2\sigma_5^2 = 0.015 \pm 0.002$ Å^2
15.1% VFF Co/Fe	$r_1 = 2.45 \pm 0.01$ Å $2\sigma_1^2 = 0.011 \pm 0.001$ Å^2	$r_2 = 2.85 \pm 0.02$ Å $2\sigma_2^2 = 0.015 \pm 0.003$ Å^2	$r_3 = 4.04 \pm 0.03$ Å $2\sigma_3^2 = 0.022 \pm 0.005$ Å^2	$r_4 = 4.72 \pm 0.04$ Å $2\sigma_4^2 = 0.023 \pm 0.006$ Å^2	$r_5 = 4.94 \pm 0.02$ Å $2\sigma_5^2 = 0.014 \pm 0.003$ Å^2
20.6% VFF Co/Fe	$r_1 = 2.47 \pm 0.01$ Å $2\sigma_1^2 = 0.011 \pm 0.001$ Å^2	$r_2 = 2.85 \pm 0.02$ Å $2\sigma_2^2 = 0.023 \pm 0.005$ Å^2	$r_3 = 4.11 \pm 0.02$ Å $2\sigma_3^2 = 0.024 \pm 0.005$ Å^2	$r_4 = 4.77 \pm 0.02$ Å $2\sigma_4^2 = 0.011 \pm 0.002$ Å^2	
28.5% VFF Co/Fe	$r_1 = 2.45 \pm 0.01$ Å $2\sigma_1^2 = 0.011 \pm 0.001$ Å^2	$r_2 = 2.84 \pm 0.02$ Å $2\sigma_2^2 = 0.023 \pm 0.003$ Å^2	$r_3 = 4.05 \pm 0.02$ Å $2\sigma_3^2 = 0.027 \pm 0.004$ Å^2	$r_4 = 4.73 \pm 0.02$ Å $2\sigma_4^2 = 0.024 \pm 0.004$ Å^2	$r_5 = 4.94 \pm 0.02$ Å $2\sigma_5^2 = 0.021 \pm 0.003$ Å^2
36.4% VFF Co/Fe	$r_1 = 2.47 \pm 0.01$ Å $2\sigma_1^2 = 0.009 \pm 0.001$ Å^2	$r_2 = 2.84 \pm 0.02$ Å $2\sigma_2^2 = 0.031 \pm 0.007$ Å^2	$r_3 = 4.08 \pm 0.02$ Å $2\sigma_3^2 = 0.028 \pm 0.005$ Å^2	$r_4 = 4.76 \pm 0.02$ Å $2\sigma_4^2 = 0.014 \pm 0.002$ Å^2	

Table 4. Structural parameters r_j, $2\sigma_j^2$ (interatomic distance, Debye–Waller factor) obtained from fits to the Fe K edge EXAFS for films of Co clusters embedded in Fe. The coordinations were fixed at values associated with the bcc structure.

	Shell 1	Shell 2	Shell 3	Shell 4	Shell 5
4.9% VFF Co/Fe	$r_1 = 2.48 \pm 0.01$ Å $2\sigma_1^2 = 0.010 \pm 0.001$ Å^2	$r_2 = 2.85 \pm 0.01$ Å $2\sigma_2^2 = 0.015 \pm 0.002$ Å^2	$r_3 = 4.07 \pm 0.01$ Å $2\sigma_3^2 = 0.020 \pm 0.003$ Å^2	$r_4 = 4.78 \pm 0.01$ Å $2\sigma_4^2 = 0.015 \pm 0.002$ Å^2	$r_5 = 4.97 \pm 0.02$ Å $2\sigma_5^2 = 0.019 \pm 0.003$ Å^2
15.1% VFF Co/Fe	$r_1 = 2.48 \pm 0.01$ Å $2\sigma_1^2 = 0.011 \pm 0.001$ Å^2	$r_2 = 2.85 \pm 0.01$ Å $2\sigma_2^2 = 0.016 \pm 0.002$ Å^2	$r_3 = 4.08 \pm 0.01$ Å $2\sigma_3^2 = 0.022 \pm 0.003$ Å^2	$r_4 = 4.79 \pm 0.01$ Å $2\sigma_4^2 = 0.017 \pm 0.003$ Å^2	$r_5 = 4.97 \pm 0.02$ Å $2\sigma_5^2 = 0.021 \pm 0.004$ Å^2
20.6% VFF Co/Fe	$r_1 = 2.48 \pm 0.01$ Å $2\sigma_1^2 = 0.011 \pm 0.001$ Å^2	$r_2 = 2.85 \pm 0.01$ Å $2\sigma_2^2 = 0.017 \pm 0.002$ Å^2	$r_3 = 4.07 \pm 0.01$ Å $2\sigma_3^2 = 0.022 \pm 0.003$ Å^2	$r_4 = 4.78 \pm 0.02$ Å $2\sigma_4^2 = 0.018 \pm 0.003$ Å^2	$r_5 = 4.97 \pm 0.02$ Å $2\sigma_5^2 = 0.020 \pm 0.004$ Å^2
28.5% VFF Co/Fe	$r_1 = 2.48 \pm 0.01$ Å $2\sigma_1^2 = 0.012 \pm 0.001$ Å^2	$r_2 = 2.85 \pm 0.01$ Å $2\sigma_2^2 = 0.019 \pm 0.002$ Å^2	$r_3 = 4.08 \pm 0.01$ Å $2\sigma_3^2 = 0.023 \pm 0.003$ Å^2	$r_4 = 4.78 \pm 0.02$ Å $2\sigma_4^2 = 0.019 \pm 0.003$ Å^2	$r_5 = 4.97 \pm 0.02$ Å $2\sigma_5^2 = 0.023 \pm 0.005$ Å^2
36.4% VFF Co/Fe	$r_1 = 2.48 \pm 0.01$ Å $2\sigma_1^2 = 0.010 \pm 0.001$ Å^2	$r_2 = 2.85 \pm 0.01$ Å $2\sigma_2^2 = 0.016 \pm 0.002$ Å^2	$r_3 = 4.07 \pm 0.01$ Å $2\sigma_3^2 = 0.021 \pm 0.002$ Å^2	$r_4 = 4.77 \pm 0.01$ Å $2\sigma_4^2 = 0.016 \pm 0.002$ Å^2	$r_5 = 4.97 \pm 0.02$ Å $2\sigma_5^2 = 0.020 \pm 0.004$ Å^2

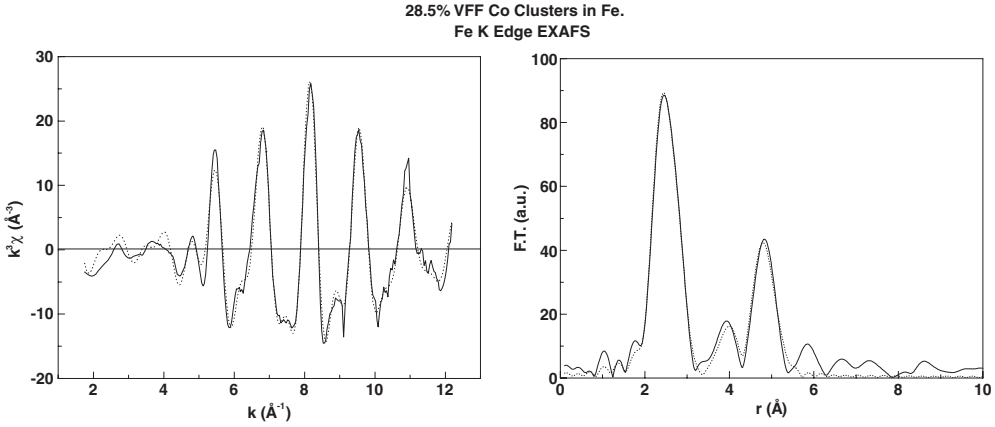

Figure 5. Fe K edge EXAFS spectrum $k^3\chi$ and Fourier transform for Fe matrix in a film containing 28.5% VFF Co clusters embedded in an Fe matrix.

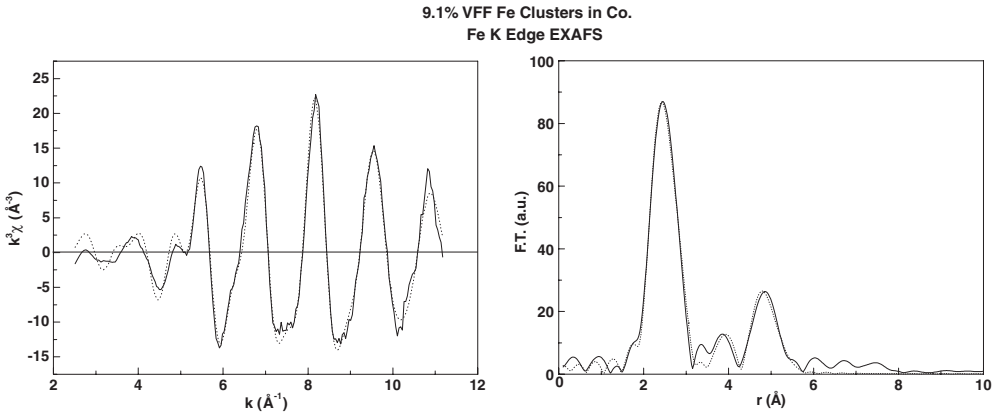

Figure 6. Fe K edge EXAFS spectrum $k^3\chi$ and Fourier transform for Fe clusters in a film containing 9.1% VFF Fe clusters embedded in a Co matrix.

composition range studied, Fe nanoclusters retain the bulk bcc structure when embedded in a Co matrix.

EXAFS data for the Co matrix are only available for the 3.9% VFF sample. Figure 7 shows the Co K edge EXAFS for this sample. It looks qualitatively very similar to the data in figure 3 for the hcp Co MBE film, and analysis confirms that the structure of the Co matrix is indeed hcp. Table 6 gives the values of r_j and σ_j^2 obtained in the fit to the data; they agree closely with the fit parameters obtained for the Co MBE film.

4. Discussion

The fit parameters for the Co edge EXAFS in table 3 clearly indicate that, when embedded in an Fe matrix, the Co clusters adopt a bcc atomic structure; this contrasts with the bulk hcp structure found for the thick Co MBE film, and also a pure Co cluster film. The values obtained in the fits for nearest-neighbour interatomic distance r_1 of 2.45 ± 0.01 Å and 2.47 ± 0.01 Å yield corresponding figures for the lattice parameter a_0 in bcc Co of 2.83 ± 0.01 Å and 2.85 ± 0.01 Å

Table 5. Structural parameters r_j, $2\sigma_j^2$ (interatomic distance, Debye–Waller factor respectively) obtained from fits to the Fe K edge EXAFS for films of Fe clusters embedded in Co. The coordinations were fixed at values associated with the bcc structure.

	Shell 1	Shell 2	Shell 3	Shell 4	Shell 5
3.9% VFF Fe/Co	$r_1 = 2.49 \pm 0.01$ Å $\sigma_1^2 = 0.011 \pm 0.001$ Å^2	$r_2 = 2.82 \pm 0.03$ Å $\sigma_2^2 = 0.061 \pm 0.010$ Å^2	$r_3 = 4.04 \pm 0.02$ Å $\sigma_3^2 = 0.037 \pm 0.005$ Å^2	$r_4 = 4.80 \pm 0.01$ Å $\sigma_4^2 = 0.025 \pm 0.002$ Å^2	
9.1% VFF Fe/Co	$r_1 = 2.49 \pm 0.01$ Å $\sigma_1^2 = 0.014 \pm 0.001$ Å^2	$r_2 = 2.83 \pm 0.01$ Å $\sigma_2^2 = 0.024 \pm 0.002$ Å^2	$r_3 = 4.04 \pm 0.02$ Å $\sigma_3^2 = 0.033 \pm 0.004$ Å^2	$r_4 = 4.75 \pm 0.02$ Å $\sigma_4^2 = 0.035 \pm 0.004$ Å^2	$r_5 = 4.98 \pm 0.02$ Å $\sigma_4^2 = 0.028 \pm 0.004$ Å^2
19.3% VFF Fe/Co	$r_1 = 2.48 \pm 0.01$ Å $\sigma_1^2 = 0.013 \pm 0.001$ Å^2	$r_2 = 2.84 \pm 0.01$ Å $\sigma_2^2 = 0.028 \pm 0.003$ Å^2	$r_3 = 4.06 \pm 0.02$ Å $\sigma_3^2 = 0.028 \pm 0.003$ Å^2	$r_4 = 4.75 \pm 0.02$ Å $\sigma_4^2 = 0.032 \pm 0.004$ Å^2	$r_5 = 4.97 \pm 0.02$ Å $\sigma_4^2 = 0.024 \pm 0.003$ Å^2

Table 6. Structural parameters r_j, $2\sigma_j^2$ (interatomic distance, Debye–Waller factor respectively) obtained from a fit to the Co K edge EXAFS for a film containing 3.9% VFF of Fe clusters embedded in Co. The coordinations were fixed at values associated with the hcp structure.

	Shell 1	Shell 2	Shell 3	Shell 4	Shell 5	Shell 6
3.9% VFF Fe/Co	$r_1 = 2.50 \pm 0.01$ Å	$r_2 = 3.53 \pm 0.02$ Å	$r_3 = 4.02 \pm 0.05$ Å	$r_4 = 4.36 \pm 0.01$ Å	$r_5 = 4.88 \pm 0.02$ Å	$r_6 = 4.99 \pm 0.02$ Å
	$2\sigma_1^2 = 0.015 \pm 0.001$ Å^2	$2\sigma_2^2 = 0.027 \pm 0.005$ Å^2	$2\sigma_3^2 = 0.019 \pm 0.011$ Å^2	$2\sigma_4^2 = 0.022 \pm 0.002$ Å^2	$2\sigma_5^2 = 0.017 \pm 0.003$ Å^2	$2\sigma_6^2 = 0.033 \pm 0.004$ Å^2

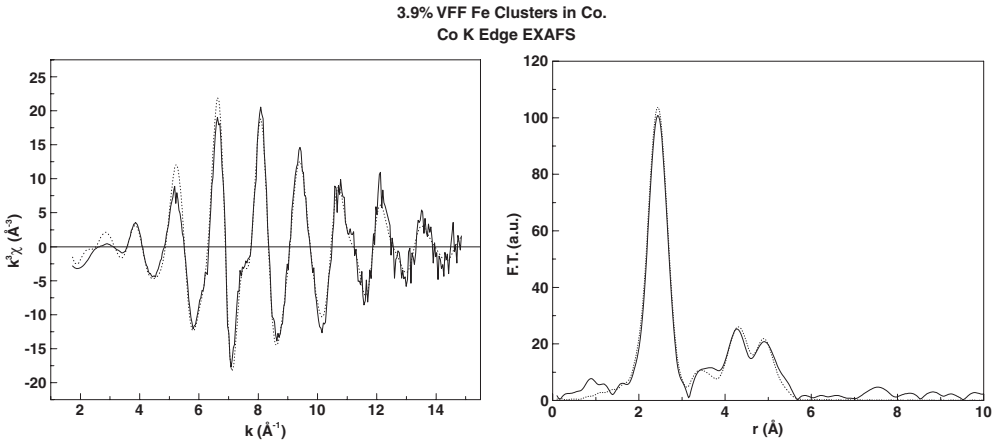

Figure 7. Co K edge EXAFS spectrum $k^3\chi$ and Fourier transform for Co matrix in a film containing 3.9% VFF Fe clusters embedded in a Co matrix.

respectively. As mentioned in section 3.2, this is less than the value in bcc Fe of 2.87 Å (the data for the Fe MBE film, presented in table 1, give $a_0 = 2.89 \pm 0.01$ Å).

It is well known that the $Fe_{1-x}Co_x$ alloy system forms a bcc structure for $0 \leqslant x < 0.75$ [26]. Progressively mixed phases are obtained for $x > 0.75$. In the bcc regime, a_0 decreases with increasing x to ∼2.83 Å for the most Co-rich bcc alloy. Comparison with the values of a_0 presented here for the Co cluster/Fe films indicates that, in going from $Fe_{0.25}Co_{0.75}$ to bcc Co, the lattice parameter does not decrease substantially further. Although we cannot rule out the possibility of some alloying at the cluster surfaces, the fact that a_0 remains unaltered across our studied composition range (in contrast to that in $Fe_{1-x}Co_x$ alloys) is consistent with a nanostructure of bcc Co clusters embedded in bcc Fe.

Reports elsewhere of bcc Co are not common. A recognition that a_0 in Co-rich $Fe_{1-x}Co_x$ alloys is close to that of a 2×2 reconstruction on GaAs led to successful attempts to grow bcc Co films by MBE on GaAs(110) [27]. From RHEED (reflection high energy electron diffraction) measurements on these films, a value for a_0 of 2.827 Å was determined. The thickest bcc Co film in [27] was 357 Å, although in subsequent efforts to grow bcc Co in this way it was found that the bcc structure usually disappears for film thicknesses around 50 Å [28], with hexagonal features appearing in the RHEED pattern. Evidence for bcc Co has also been found in Fe/Co multilayers grown by sputter deposition onto Si(111) and kapton substrates [29]. EXAFS measurements were consistent with a bcc structure in the Co layers, for Co layer thicknesses less than or equal to 30 Å, and the value reported for the Co nearest neighbour distance r_1 of 2.46 Å implies a value for a_0 of 2.84 Å. For larger thicknesses of Co layer, the structure starts to revert to hcp. More recently, bcc Co has been reported in Co cluster/Ag samples, formed by ion implantation of Co into Ag [30], although this is in contrast with other reports, which indicate that Co clusters in Ag adopt an fcc structure [16]. The authors in [30] compared measured Co K edge XANES (x-ray absorption near edge structure) spectra with spectra simulated using a full multiple-scattering *ab initio* calculation; the simulated spectra agreed well with experimental results, assuming a bcc structure in the Co clusters with $r_1 = 2.46$ Å (and hence $a_0 = 2.84$ Å). It is clear that the value of a_0 for bcc Co in our Co cluster/Fe films is in good agreement with those in the works referred to above.

Experimental verification that, under certain conditions at least, bcc Co can exist has led to a number of theoretical studies on the different structural phases of Co and other 3d transition

metals. Total energy calculations by various authors [31, 32] have shown that all three structural phases in Co (hcp, fcc, bcc) lie close to one another in energy, with bcc the highest energy phase. However, bcc Co is not a true metastable phase of bulk Co; calculations of the total energy of bcc Co as a function of various strains have found that it is unstable with respect to a volume-conserving tetragonal distortion [33] (the Bain strain [34]), which continuously transforms the bcc structure into fcc. As mentioned above, bcc structure observed in Co films [27, 28] or layers [29] collapses above a certain film or layer thickness. In our Co cluster/Fe films, the Co bcc structure is maintained up to nearly 40% VFF at least. This is significantly above the three-dimensional percolation threshold, indicating that bcc is stabilized in cluster agglomerates as well as in isolated clusters.

In addition to finding that bcc Co is not truly metastable, total energy calculations also predict that the phase should be strongly magnetic [32, 35–37] with magnetic moments comparable to or slightly greater than those in hcp Co. However, magnetometry measurements on the bcc Co films in [27] yield magnetic moments significantly less than the predicted values. Some authors have suggested that impurities and structural defects, in addition to stabilizing the bcc Co structure, may also play a role in reducing the magnetic moment [35, 36]. It is interesting to note that the bcc structure has also recently been stabilized in thin films of Ni [38], which in bulk form adopts an fcc structure at room temperature; this was achieved by MBE growth on GaAs(001). The measured atomic magnetic moment in the bcc Ni films agreed well with the value predicted by total energy calculations [32]. In the light of the above comments and total energy calculations for magnetic bcc Co, and also the work presented here, we will present and discuss the results of magnetometry measurements on our nanocomposite Co/Fe films in a forthcoming publication [21].

5. Conclusion

Co clusters embedded in an Fe matrix adopt a bcc atomic structure up to cluster concentrations of almost 40% VFF. In a pure Co cluster film, the atomic structure reverts to the hcp structure of bulk Co. Fe clusters embedded in a Co matrix retain the bulk Fe bcc structure.

Acknowledgments

The authors are grateful to Dr S Fiddy at Daresbury Laboratory for his assistance during collection of the EXAFS data. We are also grateful for support from the EC project Nanospin (contract number NMP4-CT-2004-013545).

References

[1] Billas I M L, Becker J A, Chtelain A and de Heer W A 1993 *Phys. Rev. Lett.* **71** 4067
[2] Baker S H, Binns C, Edmonds K W, Maher M J, Thornton S C, Louch S and Dhesi S S 2002 *J. Magn. Magn. Mater.* **247** 19
[3] Lau J T, Fohlisch A, Nietubye R, Rief M and Wurth W 2002 *Phys. Rev. Lett.* **89** 057201
[4] Douglass D C, Cox A J, Bucher J P and Bloomfield L A 1993 *Phys. Rev.* B **47** 12874
[5] Koboyashi S, Takahasi T and Sasaki J 1972 *J. Phys. Soc. Japan* **32** 1234
[6] Kubo R 1962 *J. Phys. Soc. Japan* **17** 975
[7] Heinz K, Bayer P and Muller S 1995 *Surf. Rev. Lett.* **2** 89
[8] Ohresser P, Brookes N B, Padovani S, Scheurer F and Bulou H 2001 *Phys. Rev.* B **64** 104429
[9] Baker S H, Roy M, Gurman S J, Louch S, Bleloch A and Binns C 2004 *J. Phys.: Condens. Matter* **16** 7813
[10] Sakurai M, Makhlouf S A, Hihara T, Sumiyama K, Wakoh K and Suzuki K 1995 *Physica* B **208/209** 614

[11] Finetti P, Dhanak V R, Binns C, Edmonds K W, Baker S H and D'Addato S 2001 *J. Electron Spectrosc. Relat. Phenom.* **114–116** 251
[12] Vergara M P C, Cezar J C, Tolentino H C N and Knobel M 2002 *Physica* B **320** 143
[13] Prieto A G, Fdez-Gubieda M L, Garcia-Arribas A, Barandiaran J M, Meneghini C and Mobilio S 2000 *J. Magn. Magn. Mater.* **221** 80
[14] Cezar J C, Tolentino H C N and Knobel M 2003 *Phys. Rev.* B **68** 0544041
[15] Cheng G, Carter J D and Guo T 2004 *Chem. Phys. Lett.* **400** 122
[16] Favre L, Stanescu S, Dupuis V, Bernstein E, Epicier T, Melinon P and Perez A 2004 *Appl. Surf. Sci.* **226** 265
[17] Benfield R E, Grandjean D, Kroll M, Pugin R, Sawitowski T and Schmid G 2001 *J. Phys. Chem.* B **105** 1916
[18] Akolekar D B, Bhargav S K, Foran G and Takahashi M 2005 *J. Mol. Catal.* A **238** 78
[19] Bazin D, Lynch J and Ramos-Fernandez M 2003 *Oil Gas Sci. Technol.—Rev. IFP* **58** 667
[20] Reifsnyder S N and Lamb H H 1999 *J. Phys. Chem.* B **103** 321
[21] Binns C, Louch S and Baker S H 2006 unpublished
[22] Baker S H, Thornton S C, Edmonds K W, Maher M J, Norris C and Binns C 2000 *Rev. Sci. Instrum.* **71** 3178
[23] Binsted N 1998 *EXCURV98: CCLRC Daresbury Laboratory Computer Program*
[24] Gurman S J, Binsted N and Ross I 1984 *J. Phys. C: Solid State Phys.* **17** 143
[25] Gurman S J and Pendry J B 1976 *Solid State Commun.* **20** 287
[26] Ellis W C and Greiner E S 1941 *Am. Soc. Met.* **29** 415
[27] Prinz G A 1985 *Phys. Rev. Lett.* **54** 1051
[28] Reidi P C, Dumelow T, Rubenstein M, Prinz G A and Qadri S B 1987 *Phys. Rev.* B **36** 4595
[29] Pizzini S, Fontaine A, Dartyge E, Giorgetti C, Baudelet F, Kappler J P, Boher P and Giron F 1994 *Phys. Rev.* B **50** 3779
[30] Zhang G, Wu Z Y, Li A, Wang Y, Zhang J, Abbas M I, Hu R, Ni X, Tong Y and Hwu Y 2004 *Phys. Rev.* B **69** 1154051
[31] Paxton A T, Methfessel M and Polatoglou H M 1990 *Phys. Rev.* B **41** 8127
[32] Guo G Y and Wang H H 2000 *Chin. J. Phys.* **38** 949
[33] Liu A Y and Singh D J 1993 *Phys. Rev.* B **47** 8515
[34] Bain E C 1924 *Trans. Am. Inst. Min. Metall. Pet. Eng.* **70** 25
[35] Marcus P M and Moruzzi V L 1985 *Solid State Commun.* **55** 971
[36] Moruzzi V L, Marcus P M, Schwarz K and Mohn P 1986 *J. Magn. Magn. Mater.* **54** 955
[37] Trygg J, Johansson B, Eriksson O and Wills J M 1995 *Phys. Rev. Lett.* **75** 2871
[38] Tian C S, Qian D, Wu D, He R H, Wu Y Z, Tang W X, Yin L F, Shi Y S, Dong G S, Jin X F, Jiang X M, Liu F Q, Qian H J, Sun K, Wang L M, Rossi G, Qiu Z Q and Shi J 2005 *Phys. Rev. Lett.* **94** 137210